Retro Models of Pt Anticancer Drug DNA Adducts: Chirality-Controlling Chelate Ligand Restriction of Guanine Dynamic Motion in (2,2′-Bipiperidine)PtG_2 Complexes (G = Guanine Derivative)

Susan O. Ano,[†] Francesco P. Intini,[‡] Giovanni Natile,*[,‡] and Luigi G. Marzilli*[,†]

Department of Chemistry, Emory University, Atlanta, Georgia 30322, and Dipartimento Farmaco-Chimico, Università degli Studi di Bari, 70125 Bari, Italy

Received December 9, 1998

Features of cisplatin-type anticancer drug adducts with nucleic acids and their constituents are clouded because they exist as a fluxional mixture of conformers. Retro-model adducts containing the specially designed chiral diamine ligand, **Bip** = 2,2′-bipiperidine, are dramatically less fluxional. Conformers of **Bip**Pt$\mathbf{G}_2$ adducts with *R,S,S,R* and *S,R,R,S* asymmetric centers at the N, C, C, and N **Bip** chelate ring atoms and **G** = 5′-GMP, 5′-dGMP, 3′-GMP, or 9-ethylguanine are amenable to separate characterization. All possible **Bip**Pt$\mathbf{G}_2$ atropisomers (one head-to-head (HH) and Δ and Λ head-to-tail (HT) atropisomers) were observed by NMR spectroscopy. At equilibrium at low pH, one HT atropisomer dominates. CD spectra, **G** H8 chemical shifts, and low-pH equilibria of **Bip**Pt$\mathbf{G}_2$ and **Me$_2$DAB**Pt$\mathbf{G}_2$ (**Me$_2$DAB** = *N,N*′-dimethyl-2,3-diaminobutane) are similar when the chelate ring atoms have the same stereochemistries; thus, **Bip** and **Me$_2$DAB** are termed chirality-controlling chelates (**CCC**) since these ligands dictate the absolute conformation of the major HT rotamer. In each case, the HT conformer that cannot form **G** O6−NH(**CCC**) hydrogen bonds was dominant, and the **G** H8 chemical shift indicated that this conformer had less tilted bases, allowing favorable base−base dipole−dipole interactions. For both the *R,S,S,R* and *S,R,R,S* **Bip** chiralities of the **BipPt**(3′-GMP)$_2$ complexes, the percentage of ΔHT rotamer increased near pH 7, a probable consequence of phosphate−cis-**G** hydrogen bonds accompanied by favorable dipole interactions of less tilted bases. For the 5′-GMP complexes, these factors favor the ΛHT rotamer near pH 7. When **G** has a 5′-phosphate group, rotamer distribution is also influenced by phosphate−NH(**Bip**) hydrogen bonds. At high pH, the nature and/or strength of interactions such as **G** dipole−**G** dipole interactions and **G** O6−NH(**Bip**) and phosphate−cis-**G** hydrogen bonding are altered by **G** N(1)H deprotonation. The features of the complexes at high pH can be largely explained as arising from the net result of these interactions. This information from retro models with a **CCC** ligand lays the foundation for understanding and evaluating the properties of the highly dynamic adducts of anticancer drugs.

Introduction

The major adduct of the anticancer drug *cis*-Pt$Cl_2(NH_3)_2$ (cisplatin) with DNA, the molecular target, is an adjacent intrastrand d(G*pG*) cross-link (G* = N7-platinated guanosine in an oligonucleotide or nucleic acid).[1−3] This cross-link is usually thought to have only the head-to-head (HH) conformation (Chart 1).[3−13] Recently several different HH models of the d(G*pG*) cross-link structure in DNA and oligonucleotide duplexes have been advanced, with the 5′-G* involved in Watson−Crick base pairing in some structural models but not in others.[14] Base pairing is clearly disrupted in the less common interstrand cross-links, which are formed by cisplatin most frequently at a d(GpC) DNA sequence and are designated as d(G*−G*).[15,16] The d(G*−G*) adducts have a head-to-tail (HT) conformation (Chart 1).[15,16]

Although we discuss other structural aspects below, we focus initially on the Pt(guanine base)$_2$ moiety (Chart 1). There are two HT base orientations that differ in chirality; the related conformers are named ΔHT and ΛHT (Chart 1).[17,18] It should

[†] Emory University.
[‡] Università degli Studi di Bari.

(1) Reedijk, J. *J. Chem. Soc., Chem. Commun.* **1996**, 801.
(2) Takahara, P. M.; Rosenzweig, A. C.; Frederick, C. A.; Lippard, S. J. *Nature* **1995**, *377*, 649.
(3) Takahara, P. M.; Frederick, C. A.; Lippard, S. J. *J. Am. Chem. Soc.* **1996**, *118*, 12309.
(4) Fouts, C. S.; Marzilli, L. G.; Byrd, R. A.; Summers, M. F.; Zon, G.; Shinozuka, K. *Inorg. Chem.* **1988**, *27*, 366.
(5) Berners-Price, S. J.; Frenkiel, T. A.; Ranford, J. D.; Sadler, P. J. *J. Chem. Soc., Dalton Trans.* **1992**, 2137.
(6) Sherman, S. E.; Gibson, D.; Wang, A. H.-J.; Lippard, S. J. *Science (Washington, D.C.)* **1985**, *230*, 412.
(7) Mukundan, S., Jr.; Xu, Y.; Zon, G.; Marzilli, L. G. *J. Am. Chem. Soc.* **1991**, *113*, 3021.
(8) Caradonna, J. P.; Lippard, S. J. *Inorg. Chem.* **1988**, *27*, 1454.
(9) Neumann, J.-M.; Tran-Dinh, S.; Girault, J.-P.; Chottard, J.-C.; Huynh-Dinh, T. *Eur. J. Biochem.* **1984**, *141*, 465.
(10) Kline, T. P.; Marzilli, L. G.; Live, D.; Zon, G. *J. Am. Chem. Soc.* **1989**, *111*, 7057.
(11) den Hartog, J. H. J.; Altona, C.; van Boom, J. H.; van der Marel, G. A.; Haasnoot, C. A. G.; Reedijk, J. *J. Biomol. Struct. Dyn.* **1985**, *2*, 1137.
(12) Admiraal, G. A.; van der Veer, J.; de Graff, R. A.; den Hartog, J. H. J.; Reedijk, J. *J. Am. Chem. Soc.* **1987**, *109*, 592.
(13) Ano, S. O.; Intini, F. P.; Natile, G.; Marzilli, L. G. *J. Am. Chem. Soc.* **1998**, *120*, 12017.
(14) Ano, S. O.; Kuklenyik, Z.; Marzilli, L. G. In *Cisplatin: Chemistry and Biochemistry of a Leading Anticancer Drug*; Lippert, B., Ed.; Wiley-VCH: Weinheim, 1999; pp 247−291.
(15) Huang, H.; Zhu, L.; Reid, B. R.; Drobney, G. F.; Hopkins, P. B. *Science (Washington, D.C.)* **1995**, *270*, 1842.
(16) Paquet, F.; Pérez, C.; Leng, M.; Lancelot, G.; Malinge, J.-M. *J. Biomol. Struct. Dyn.* **1996**, *14*, 67.

10.1021/ic981409g CCC: $18.00
Published on Web 05/22/1999

Chart 1. Sketches of the HT Rotamers of (*S,R,R,S*)- and (*R,S,S,R*)-**Bip**Pt**G**$_2$ with Left-Handed and Right-Handed Tilt, Respectively[a]

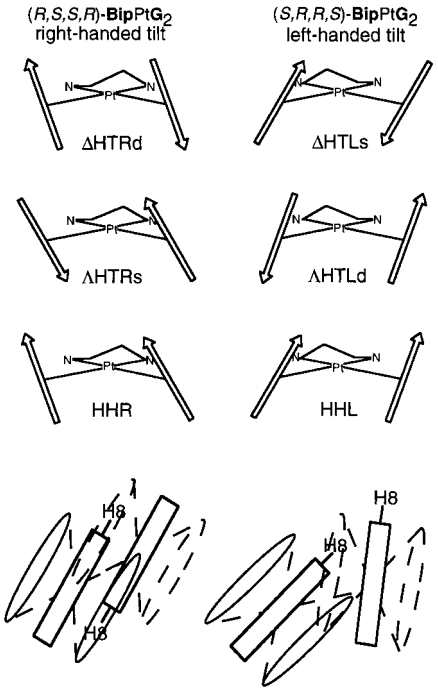

[a] Arrows represent N7-bound **G**, with the head of the arrow representing the H8 atom; the HT chiralities are described in the text. The bulk of the **Bip** ligand, shown in Chart 3, has been omitted for clarity. The d and s notations for the less tilted and more tilted subforms indicate that the H8's of these subforms are relatively deshielded and shielded, respectively. The sketches at the bottom depict examples of the effect of the shielding cones of the **G** bases; Both H8's are shielded in the ΔHTLs Subform (left), and only one H8 is shielded in the HHL subform (right).

Chart 2. Schematic Representation of Guanine Derivatives (**G**), with the Atom-Numbering Scheme for the Base

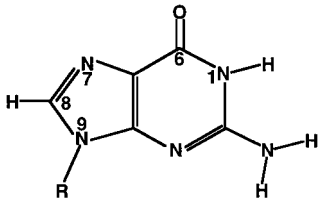

be noted that since the guanine N9 substituent is usually chiral, the ΔHT and ΛHT conformers are normally not a pair of enantiomers. For simple *cis*-PtA_2**G**$_2$ cross-link models (A_2 = a diamine or two amines; **G** = a guanine derivative, Chart 2) with C_2-symmetrical PtA_2 moieties (including resolved chiral A_2 carrier ligands), the three guanine arrangements lead to three conformers. (More conformers are possible for unsymmetrical A_2 ligands or when the G's are tethered by a sugar phosphate backbone.) Although until recently[13,19] only the HH and the ΔHT arrangements have been found for the respective d(G*pG*) and d(G*−G*) cross-links,[14] our work has shown that there is greater conformational diversity than previously predicted.

In the present study, we do not discuss conformational diversity resulting from the N9 substituent and the phosphodiester linkage since these considerations are not relevant to simple *cis*-PtA_2**G**$_2$ cross-link models with unconnected identical **G**'s. Cumulative evidence, mainly from solid state data, indicates that in all adducts the bases have either a small tilt or a large tilt. Although various other tilt combinations can be conceived, the literature suggests that six (referred to here as subforms) are preferred (Chart 1); there are left-handed or right-handed subforms for each conformer.[14,20]

In solution, the situation is not so clear since the subforms are easily interchanged by facile rotation about the Pt−N7 single bond. We call the following collective complications the dynamic motion problem. The dynamic nature of the *cis*-PtA_2**G**$_2$ adducts when A_2 is $(NH_3)_2$ or has two primary amine donors makes understanding of solution conformation and dynamics difficult. The unsymmetrical nature of the d(G*pG*) cross-links means that each nucleus is unique and that one NMR signal will be observed in the cases of either two or more forms interchanging by fast dynamic motion or of a relatively static form. For simple adducts with untethered **G**'s, the **G** rotation rate is too fast on the NMR time scale to permit observation of the **G** H8 singlets of different conformers in the ^{1}H NMR spectrum; a single H8 signal representing an average of all possible conformers is normally observed. Thus, there is no direct evidence for the widely held belief that these simple dynamic adducts exist as a nearly equal mixture of the two HT conformers,[21] nor indeed is it clear what subforms are present. However, studies using bulky A_2 ligands (see below), adenine nucleotides,[22] and metal ion trapping of rotating **G** nucleotides[23] all suggest that in solution both HT conformers are nearly equally stable and dominate over the HH conformer. In contrast, complexes with **G** nucleosides and nucleotides show that the ΔHT conformer dominates in the solid state to essentially the complete exclusion of the other conformers.[24−29]

In most modeling of biological/medical systems, simple models are introduced to overcome the complexity of the system. In contrast, cisplatin is one of the simplest molecules of great clinical importance. Its simplicity complicates its study. Thus, we introduce the term "retro-modeling" to stress the point that we are building more elaborate, not less elaborate, analogues of the relevant species.

Bulky A_2 ligands hinder **G** rotation about the Pt−N7 bond; the first evidence of *cis*-PtA_2**G**$_2$ HT rotamers in solution was obtained in the classic work of Cramer.[17,30] Both HT forms were present in equal amounts, but no HH form was evident; however, the ligand used, *N,N,N′,N′*-tetramethylethylenediamine, lacked the NH groups found to be important in anticancer activity.[17,30] In our retro-modeling, we decided to use carrier ligands with bulky secondary amine donors (Chart 3). These have the advantage of possessing an NH group but the disadvantage that the secondary N could adopt one of two asymmetric configura-

(17) Cramer, R.; Dahlstrom, P. *Inorg. Chem.* **1985**, *24*, 3420.
(18) Williams, K. M.; Cerasino, L.; Intini, F. P.; Natile, G.; Marzilli, L. G. *Inorg. Chem.* **1998**, *37*, 5260.
(19) Unpublished results from these laboratories.
(20) Kozelka, J.; Fouchet, M. H.; Chottard, J.-C. *Eur. J. Biochem.* **1992**, *205*, 895.
(21) Sinur, A.; Grabner, S. *Acta Crystallogr. C* **1995**, *51*, 1769.
(22) Reily, M. D.; Marzilli, L. G. *J. Am. Chem. Soc.* **1986**, *108*, 6785.
(23) Isab, A.; Marzilli, L. G. *Inorg. Chem.* **1998**, *37*, 6558.
(24) Gellert, R. W.; Bau, R. *J. Am. Chem. Soc.* **1975**, *97*, 7379.
(25) Cramer, R. E.; Dahlstrom, P. L.; Seu, M. J. T.; Norton, T.; Kashiwagi, M. *Inorg. Chem.* **1980**, *19*, 148.
(26) Miller, S. K.; van der Veer, D. G.; Marzilli, L. G. *J. Am. Chem. Soc.* **1985**, *107*, 1048.
(27) Marzilli, L. G.; Chalilpoyil, P.; Chiang, C. C.; Kistenmacher, T. J. *J. Am. Chem. Soc.* **1980**, *102*, 2480.
(28) Orbell, J. D.; Taylor, M. R.; Birch, S. L.; Lawton, S. E.; Vilkins, L. M.; Keefe, L. J. *Inorg. Chim. Acta* **1988**, *152*, 125.
(29) Barnham, K. J.; Bauer, C. J.; Djuran, M. I.; Mazid, M. A.; Rau, T.; Sadler, P. J. *Inorg. Chem.* **1995**, *34*, 2826.
(30) Cramer, R. E.; Dahlstrom, P. L. *J. Am. Chem. Soc.* **1979**, *101*, 3679.

Chart 3. Sketches of the **Bip**Pt (Top), **Me$_2$DAB**Pt (Middle), and **pipen**Pt (Bottom) Moieties with the *S,R,R,S* or *S,R* Chiralities on the Right and the *R,S,S,R* or *R,S* Chiralities on the Left

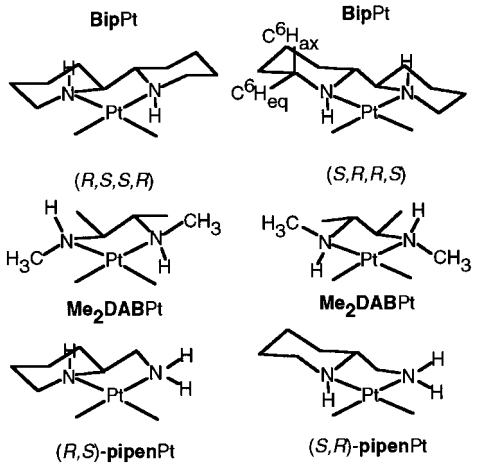

tions. We approached this problem by designing chirality into the chelate ring in order to control the amine chirality[18,31−36] and have emphasized C_2-symmetrical diamines with *R,S,S,R* or *S,R,R,S* asymmetric centers at N, C, C, and N chelate ring atoms (Chart 3).[31,34,36] In our first retro-modeling studies, with the **Me$_2$DAB** (*N,N′*-dimethyl-2,3-diaminobutane) carrier ligand (Chart 3), we observed for the first time NMR evidence for the HH atropisomer of a simple *cis*-PtA_2**G**$_2$ model in solution.[31] The HH form was a minor species, and the two HT forms could also be observed.

These cross-link retro models with slow dynamic motion are allowing us to assess many properties of adducts that were obscured by the dynamic motion problem. For example, the results agree with the solid state evidence indicating that (a) untethered **G**'s adopt an HT conformation in preference to the HH conformation and (b) tethered **G**'s linked by a sugar phosphate backbone adopt the HH conformation. It appears that the HH form has some energetically unfavorable features in *cis*-PtA_2**G**$_2$ complexes. In contrast, the HH form is dominant in Re and Ru benzimidazole complexes.[37−39] These systems have a ligated imidazole ring, such as that in purine nucleobases; the conformation is clearly dictated to a large extent by an electrostatic attraction of the partially positively charged N_2-CH proton to the cis negative ligands.[39] In contrast to these octahedral complexes, the square planar cis-type Pt drugs have no cis negative ligands to interact with the **G** H8 atoms, and the factors dictating the HH conformation in d(G*pG*) adducts are not so clear. Part of our goal is to understand factors influencing conformation, especially when the **G** bases are part of oligonucleotides or DNA.

Although informative, this **Me$_2$DAB** system has limitations since the rotamers proved to be fluxional, interconverting rapidly via rotation about the Pt−N7 bond even below room temperature, as evidenced by broad signals and EXSY peaks in the NOESY spectra.[34] Improvement in ligand design led to use of the ligand **Bip** (2,2′-bipiperidine, Chart 3). Like **Me$_2$DAB**, **Bip** has two preferred C_2-symmetric coordinated configurations with *R,S,S,R* or *S,R,R,S* asymmetric centers (Chart 3).[36] Since the **Bip** NH's are contained in a ligand ring in addition to the chelate ring, **Bip** is more resistant than **Me$_2$DAB** to base-catalyzed inversion of N chirality. Nevertheless, the bulk of the **Bip** ligand is concentrated near the Pt coordination plane, a feature that leads to a rotamer distribution at equilibrium similar to that of **Me$_2$DAB** complexes. We found that carrier ligand chirality influences whether a ΔHT or ΛHT conformer dominates;[34,36] these A_2 ligands are called chirality-controlling chelate (**CCC**) ligands.[34] The major HT rotamer of (*R,S,S,R*)-(**CCC**)Pt(5′-GMP)$_2$ and (*S,R,R,S*)-(**CCC**)Pt(5′-GMP)$_2$ had the Δ and Λ chirality, respectively. (Note that we designate the carrier ligand class and the abbreviation **CCC** in boldface to distinguish the ligand from cytidine.)

In **Me$_2$DAB**, the *N*-methyl groups imparting the bulk can rotate freely; however, the equivalently placed methylene groups of **Bip** are relatively rigid, a feature designed to slow equilibration of the **Bip** adducts. Thus, we were able to examine the products of the coordination step for the second **G** in the reaction of **Bip**Pt with 5′-GMP at low pH before the products had time to redistribute.[36] We found the initial distribution to be that expected from statistics, namely, ∼50% HH adduct and ∼25% of each HT adduct. With time, equilibration occurred and the HH rotamer became a minor species. We have succeeded in minimizing the dynamic motion problem by slowing the dynamic Pt−N7 bond rotation by a factor of $\sim 10^6-10^7$ compared to the active drugs.

Pt−N7 bond rotation has been proposed to be critical in the formation of cross-link lesions when cis-type Pt drugs react with DNA.[22,30,40−43] Long-lived mono adducts in platinated duplexes have been identified in which the Pt−Cl bond may be shielded from hydrolysis by interactions between the duplex and the Pt ligand.[44] Thus, rotation is necessary to allow hydrolysis of the second Cl. There is a growing belief that slow reaction rates may alter adduct distribution and affect anticancer activity.[45] Minor cross-links involve both A and G; recent studies have attributed the differences in the distribution of cross-link adducts to differences in reaction rates associated with the larger size of the adenine 6-amino group compared to the **G** O6 group.[46] The slow rotation observed with simple complexes of adenine nucleotides has been explained similarly.[22] However, alternative explanations have been advanced.[47,48]

(31) Xu, Y.; Natile, G.; Intini, F. P.; Marzilli, L. G. *J. Am. Chem. Soc.* **1990**, *112*, 8177.
(32) Wong, H. C.; Intini, F. P.; Natile, G.; Marzilli, L. G. *Inorg. Chem.* **1999**, *38*, 1006.
(33) Wong, H. C.; Coogan, R.; Intini, F. P.; Natile, G.; Marzilli, L. G. *Inorg. Chem.* **1999**, *38*, 777.
(34) Marzilli, L. G.; Intini, F. P.; Kiser, D.; Wong, H. C.; Ano, S. O.; Marzilli, P. A.; Natile, G. *Inorg. Chem.* **1998**, *37*, 6898.
(35) Kiser, D.; Intini, F. P.; Xu, Y.; Natile, G.; Marzilli, L. G. *Inorg. Chem.* **1994**, *33*, 4149.
(36) Ano, S. O.; Intini, F. P.; Natile, G.; Marzilli, L. G. *J. Am. Chem. Soc.* **1997**, *119*, 8570.
(37) Marzilli, L. G.; Iwamoto, M.; Alessio, E.; Hansen, L.; Calligaris, M. *J. Am. Chem. Soc.* **1994**, *116*, 815.
(38) Alessio, E.; Hansen, L.; Iwamoto, M.; Marzilli, L. G. *J. Am. Chem. Soc.* **1996**, *118*, 7593.
(39) Marzilli, L. G.; Marzilli, P. A.; Alessio, E. *Pure Appl. Chem.* **1998**, *70*, 961.
(40) Dijt, F. J.; Canters, G. W.; den Hartog, J. H. J.; Marcelis, A. T. M.; Reedijk, J. *J. Am. Chem. Soc.* **1984**, *106*, 3644.
(41) Marcelis, A. T. M.; van Kralingen, C. G.; Reedijk, J. *J. Inorg. Biochem.* **1980**, *13*, 213.
(42) Marcelis, A. T. M.; Korte, H.-J.; Krebs, B.; Reedijk, J. *Inorg. Chem.* **1982**, *21*, 4059.
(43) Miller, S. K.; Marzilli, L. G. *Inorg. Chem.* **1985**, *24*, 2421.
(44) Berners-Price, S. J.; Barnham, K. J.; Frey, U.; Sadler, P. J. *Chem.—Eur. J.* **1996**, *2*, 1283.
(45) Fichtinger-Schepman, A. M. J.; Welters, M. J. P.; van Dijk-Knijnenburg, H. C. M.; van der Sterre, M. L. T.; Tilby, M. J.; Berends, F.; Baan, R. A. In *Platinum and Other Metal Coordination Compounds in Cancer Chemotherapy 2*; Pinedo, H. M., Schornagel, J. H., Eds.; Plenum Press: New York, 1996; p 107.
(46) Davies, M. S.; Berners-Price, S. J.; Hambley, T. W. *J. Am. Chem. Soc.* **1998**, *120*, 11380.

The study of these **Bip** retro models has advanced our goals of elucidating the fundamental factors influencing structure, dynamics, and energetics of *cis*-Pt-type adducts formed by active drugs. Here we examine the adducts with 5′-GMP,[49] 5′-dGMP, 3′-GMP, and 9-EtG. Work in progress focuses on oligonucleotides.

Experimental Section

Materials. 5′-GMP, 5′-dGMP, 3′-GMP, and 9-EtG (Aldrich) were used as received. (*R,S,S,R*)-**Bip**Pt$(NO_3)_2$, (*S,R,R,S*)-**Bip**Pt$(NO_3)_2$, (*R,S,S,R*)-**Bip**Pt$(H_2O)(SO_4)$, (*S,R,R,S*)-**Bip**Pt$(H_2O)(SO_4)$, or an unresolved mixture of the enantiomers was utilized. Preparation of the **Bip**Pt complexes has been described.[13,19]

Methods. Typical preparations [2−3 equiv of **G** with 1 equiv, ∼10−20 mM, of [**Bip**Pt$(H_2O)_2]^{2+}$ in D_2O (0.5−1.0 mL) at pH 3 (or pH 7)] were monitored by ^{1}H NMR spectroscopy. When either no free **G** H8 signal or no change in H8 signal intensity was observed, samples were studied. Samples for 2D NMR experiments were eventually lyophilized and redissolved in 99.96% D_2O.

^{1}H NMR spectra, obtained on GE GN-Omega 600 or Varian Unity+500 spectrometers, were referenced to the residual HOD peak.[50] Saturation transfer experiments used a 16K block size and presaturation pulse sequence. Symmetrical irradiations were done flanking the peak of interest to eliminate power spillage effects. 2D NMR data [256 (or 512) × 2048 matrix] were collected using a spectral width of 6250 Hz and were processed using Felix 2.3 (Molecular Simulations, Inc.).

2D phase sensitive NOESY[49] data[51−53] were collected at 5 °C for *rac*-**Bip**Pt(5′-GMP)$_2$ with 32 scans per t_1 increment and a 300 ms mixing time. Each acquisition included a 2.6 s presaturation pulse and 10 ms delay. Data were processed using an exponential apodization function with a line broadening of 2 Hz in t_2, while a 90° phase-shifted sine bell over 256 points was used in t_1. The evolution dimension was zero-filled to 2K points prior to Fourier transformation.

A 2D DQF COSY experiment[54] was performed at 25 °C for *rac*-**Bip**Pt(5′-GMP)$_2$ with 96 scans per t_1 increment. Each acquisition included a 1.6 s presaturation pulse and 10 ms delay. Data were apodized by using an exponential multiplication with a line broadening of 1 Hz in t_2 and a 90° phase-shifted squared sine bell along 256 points in t_1. The evolution dimension was zero-filled to 2K prior to Fourier transformation and the first point multiplied by 0.5.

2D ROESY experiments[55−57] were performed for [(*R,S,S,R*)-**Bip**Pt-(9-EtG)$_2]^{2+}$ at 5 °C using mixing times of 100 (64 scans per t_1 increment) and 350 ms (48 scans per t_1 increment). Each acquisition included a 0.5 s presaturation pulse and a 1.5 s (2.5 s for 350 ms mixing time) delay. In both experiments, a time-shared spin-lock field with an effective field strength of 4000 Hz was implemented. Spectra were apodized using a 90° phase-shifted sine bell over 2048 points in t_2, and a 90° phase-shifted squared sine bell in t_1. The evolution dimension was zero-filled to 2K prior to Fourier transformation and the first point multiplied by 0.5.

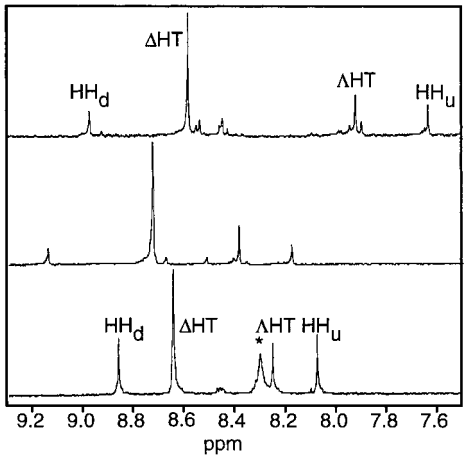

Figure 1. H8 ^{1}H NMR signals of (*R,S,S,R*)-**Bip**Pt(5′-GMP)$_2$ at (from bottom to top) pH 3, 7.6, and 12, 25 °C. Small peaks in these and later figures most probably arise from monoadducts. The pH 3 spectrum was collected before equilibrium was reached; ∗ indicates free 5′-GMP.

CD samples (∼27 μM) were prepared by diluting aliquots from NMR samples when available; otherwise, equilibrium samples were prepared by adding [**Bip**Pt$(H_2O)_2]^{2+}$ and **G** from stock solutions in a 1:2−3 ratio to 3 mL of deionized H_2O at pH ∼3. To ensure completeness of reaction, the solutions were stored at 15 °C in the dark for at least 2 days before spectral acquisition.

Molecular mechanics and dynamics (MMD) calculations were carried out using the Discover (version 2.9 or 94) module of the InsightII package (MSI) on a Silicon Graphics Indy workstation with our recently developed force field.[58] Charges on the **Bip** ligand were determined using the CFF91 force field and corrected for the positive charge from Pt as described.[58] Minimization included 1000 cycles of steepest descents and 5000 cycles of conjugate gradient until a Δ rms gradient of 0.0001 kcal/(mol·Å) was obtained. Dynamics runs were preceded by minimization and consisted of a 500 ps constant temperature simulation at 300 K. The conformers were sampled every 1 ps, and the resulting 500 structures were minimized to a Δ rms gradient of 0.001 kcal/(mol·Å). For MMD calculations, the distance-dependent dielectric constant was set to $4r_{ij}$, while 1−4 nonbonded interactions were scaled by a factor of 0.5.

Results

(*R,S,S,R*)-BipPt(5′-GMP)$_2$ and (*S,R,R,S*)-BipPt(5′-GMP)$_2$. At equilibrium, (*R,S,S,R*)-**Bip**Pt(5′-GMP)$_2$ at pH 3 and 25 °C had four H8 ^{1}H NMR signals (Figure 1). One signal accounted for more than 50% of the total H8 area and, in the absence of a partner signal, was assigned to an HT rotamer. Three atropisomers were also observed for (*S,R,R,S*)-**Bip**Pt(5′-GMP)$_2$ at pH 3 (Figure 2). Again, one H8 signal dominated the region of the spectrum at equilibrium and was assigned to an HT atropisomer. The most downfield (HH$_d$) and most upfield (HH$_u$) H8 signals of (*R,S,S,R*)-**Bip**Pt(5′-GMP)$_2$ and (*S,R,R,S*)-**Bip**Pt-(5′-GMP)$_2$ were assigned to the respective HH atropisomer on the basis of equal integration and of the similarity of both of the shift values and the ∼1 ppm separation to those of the signals of the HH form of the analogous (*R,S,S,R*)- and (*S,R,R,S*)-**Me$_2$DAB**Pt(5′-GMP)$_2$ complexes.[31,34]

2D NMR Methods for Determining Conformation. The NH, C^6H_{ax}, and C^6H_{eq} (Chart 3) signals, assigned using 2D NMR spectroscopy at 5 °C, were used to determine the absolute conformations of the rotamers. The 1D ^{1}H NMR spectrum of *rac*-**Bip**Pt(5′-GMP)$_2$ at 5 °C contained the same eight H8 signals in similar ratios as observed at 25 °C (Table 1). The method for assigning the absolute conformation of the HT atropisomers involves measurement and comparison of the volumes of the

(47) Li, D.; Bose, R. N. *J. Chem. Soc., Chem. Commun.* **1992**, 1596.
(48) Li, D.; Bose, R. N. *J. Chem. Soc., Dalton Trans.* **1994**, 3717.
(49) Abbreviations: 5′-GMP = guanosine 5′-monophosphate; 5′-dGMP = deoxyguanosine 5′-monophosphate; 3′-GMP = guanosine 3′-monophosphate; 9-EtG = 9-ethylguanine; NOESY = nuclear Overhauser enhancement spectroscopy; DQF COSY = double-quantum filtered correlation spectroscopy; ROESY = rotating frame Overhauser enhancement spectroscopy.
(50) Brabec, V.; Sip, M.; Leng, M. *Biochemistry* **1993**, *32*, 11676.
(51) Jeener, J.; Meier, B. H.; Bachmann, P.; Ernst, R. R. *J. Chem. Phys.* **1979**, *71*, 4546.
(52) Kumar, A.; Ernst, R. R.; Wüthrich, K. *Biochem. Biophys. Res. Commun.* **1980**, *95*, 1.
(53) States, D. J.; Haberkorn, R. A.; Ruben, D. J. *J. Magn. Reson.* **1982**, *48*, 286.
(54) Bodenhausen, G. *Prog. Nucl. Magn. Reson. Spectrosc.* **1981**, *14*, 137.
(55) Bothner-By, A. A.; Stephens, R. L.; Lee, J.-M. *J. Am. Chem. Soc.* **1984**, *106*, 811.
(56) Bax, A.; Davis, D. G. *J. Magn. Reson.* **1985**, *63*, 207.
(57) Griesinger, C.; Ernst, R. R. *J. Magn. Reson.* **1987**, *75*, 261.
(58) Yao, S.; Plastaras, J. P.; Marzilli, L. G. *Inorg. Chem.* **1994**, *33*, 6061.

Table 1. Assignments of H8, NH, C^2H, C^6H_{ax}, and C^6H_{eq} Signals for the Atropisomers of (*R,S,S,R*)-**Bip**Pt(5′-GMP)$_2$ and (*S,R,R,S*)-**Bip**Pt(5′-GMP)$_2$ from 5 °C NOESY, DQF COSY, and 1D Data at pH 3.0 (Blanks Indicate no Assignment)

H8	**Bip** confign	H8 (ppm)	NH (ppm)	H8−NH cross-peak vol[a]	C^6H_{ax} (ppm)	H8−C^6H_{ax} cross−peak vol[a]	C^2H (ppm)	C^6H_{eq} (ppm)	H8−C^6H_{eq} cross−peak vol[a]
HH_u	*R,S,S,R*	8.11	∼5.8		2.73		2.50	2.48	
ΛHT	*R,S,S,R*	8.30	5.41[b]		2.80		2.55	2.53	
ΔHT	*R,S,S,R*	8.71	6.31	78	2.78	5	2.65	2.55	99
HH_d	*R,S,S,R*	8.90	6.26	10	2.80		2.67	2.26	
HH_u	*S,R,R,S*	8.06	∼5.5[b]						
ΔHT	*S,R,R,S*	8.33	5.46[b]		2.82				
ΛHT	*S,R,R,S*	8.51	6.17	11	2.75	1	2.67	2.40	45
HH_d	*S,R,R,S*	8.91	6.47	6	2.66	3	2.28	2.26	31

[a] Volumes were divided by the smallest volume found (H8 signal $C-C^6H_{ax} = 1$). [b] Assignment not clear based on 2D spectra. No H8−NH cross-peaks found in NOESY spectrum but NH signals clearly present in 1D spectrum. These NH's in the 1D spectrum were not assignable to any other signals based on 2D data.

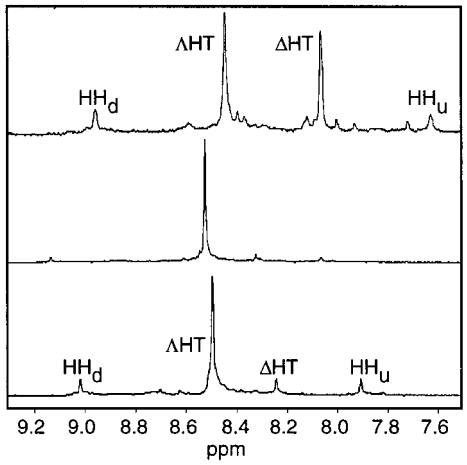

Figure 2. H8 ^1H NMR signals of (*S,R,R,S*)-**Bip**Pt(5′-GMP)$_2$ at (from bottom to top) pH 3, 7.4, and 11, 25 °C.

H8−NH and H8−C^6H_{ax} NOE cross-peaks. If the relative ratio (volume of H8−NH cross-peak: volume of H8−C^6H_{ax} cross-peak) is >1, the 5′-GMP is oriented with the H8 on the same side of the platinum coordination plane as the NH. If this ratio is <1, the 5′-GMP is oriented with the H8 on the opposite side of the platinum coordination plane from the NH. Strong NOE cross-peaks were observed from the four most downfield H8 signals to NH, and three of these H8 signals also had NOE cross-peaks to C^6H_{eq} signals (Table 1). Small H8−C^6H_{ax} NOE cross-peaks were observed in a few cases, indicating a long distance. Therefore, the absolute conformations of the major HT rotamers at low pH of (*R,S,S,R*)-**Bip**Pt(5′-GMP)$_2$ and (*S,R,R,S*)-**Bip**Pt(5′-GMP)$_2$ were assigned as ΔHT and ΛHT, respectively.

The conformation and the signal assignments of the HH atropisomers determined above by 1D NMR spectroscopy were confirmed through cross-peaks between their H8 signals (Supporting Information). No exchange phenomena were observed in the 2D NOESY spectrum. In contrast, exchange between the rotamers of **Me$_2$DAB**Pt(5′-GMP)$_2$ was observed even at 5 °C.[31,34]

Saturation Transfer Experiments. Since exchange processes are favored at high temperature, 1D saturation transfer experiments were done at 30, 60, or 80 °C. For (*R,S,S,R*)- and (*S,R,R,S*)-**Bip**Pt(5′-GMP)$_2$, no magnetization transfer was observed between any atropisomers.

pH Studies. There are three ionizable groups on 5′-GMP: (a) the phosphate group (pK_a 5.8−6.1 vs 6.2 for free 5′-GMP);[18,33] (b) **G** N(1)H (pK_a ∼8.5 for platinated nucleotides);[59−61] and (c) ribose OH (pK_a ∼12.5).[62] Because Pt binding withdraws electron density from the **G** base, the pK_a value for N(1)H is lower compared to unplatinated **G**. Upon deprotonation of the phosphate group, the H8 signals usually experience a downfield shift of ∼0.2 ppm.[40,63] When N(1)H is deprotonated, the H8 signals either do not shift[18] (a rare observation) or shift upfield (commonly observed).[34,40,61,64]

Table 2. Major:Minor HT Ratio for (*R,S,S,R*)-**Bip**Pt**G**$_2$ (Δ:Λ) and (*S,R,R,S*)-**Bip**Pt**G**$_2$ (Λ:Δ) Complexes as a Function of pH

	R,S,S,R			*S,R,R,S*		
G	pH 3	pH 7	pH 11−12	pH 3	pH 7	pH 11−12
5′-GMP	4.8	3.3	3.3	6.5	>25	<1
5′-dGMP				7	>25	
3′-GMP	7.2	20	1.2	3.5	1.4	<1
9-EtG (*rac*)	1.5	1.5	0.5			

For (*R,S,S,R*)-**Bip**Pt(5′-GMP)$_2$, the major:minor HT ratio decreased slightly from ∼4.8 at pH 3 to ∼3.3 at pH 7 (Table 2). The HH H8 signals each decreased in intensity. These changes were maintained for 40 days with no additional peaks appearing, indicating no isomerization or degradation of the coordinated **Bip** ligand. Lowering the pH to 3 restored the low-pH ^1H NMR intensities and hence equilibrium populations. At pH 7, the H8 signals shifted downfield (∼0.3, 0.1, 0.13, and 0.06 ppm for the HH_d, major HT, minor HT, and HH_u H8 signals, respectively). From pH 7.4 to 11, the major:minor HT ratio did not change significantly (Figure 1 and Table 2). The HH_u and ΛHT H8 signals, the H8 signals from **G** bases that can have O6−NH hydrogen bonds, shifted upfield more than did the HH_d and ΔHT H8 signals over this pH range. There was no significant shift of the H1′ or H2′ signals, suggesting no 2′-OH deprotonation.

For (*S,R,R,S*)-**Bip**Pt(5′-GMP)$_2$, the ΛHT atropisomer dominated at all pH values except at very high pH, where the ΛHT and ΔHT atropisomers were comparable. At pH 3, the major:minor HT ratio was ∼6.5 (Table 2), but at pH 7.4, the H8 region was dominated almost exclusively by the ΛHT H8 signal (major:minor HT ratio > 25) (Figure 2 and Table 2). This prevalence was maintained for 21 days, over which time no new peaks appeared. The original population ratio at low pH was restored upon lowering the pH to 3. At pH 7, all of the H8 signals shifted downfield; both HH H8 signals shifted more

(59) Chu, G. Y. H.; Mansy, S.; Duncan, R. E.; Tobias, R. S. *J. Am. Chem. Soc.* **1978**, *100*, 593.
(60) Chottard, J.-C.; Girault, J.-P.; Chottard, G.; Lallemand, J.-Y.; Mansuy, D. *J. Am. Chem. Soc.* **1980**, *102*, 5565.
(61) Girault, J.-P.; Chottard, G.; Lallemand, J.-Y.; Chottard, J.-C. *Biochemistry* **1982**, *21*, 1352.
(62) Saenger, W. *Principles of Nucleic Acid Structure*; Springer-Verlag: New York, 1984; p 1.
(63) Martin, R. B. *Acc. Chem. Res.* **1985**, *18*, 32.
(64) Caradonna, J. P.; Lippard, S. J.; Gait, M. J.; Singh, M. *J. Am. Chem. Soc.* **1982**, *104*, 5793.

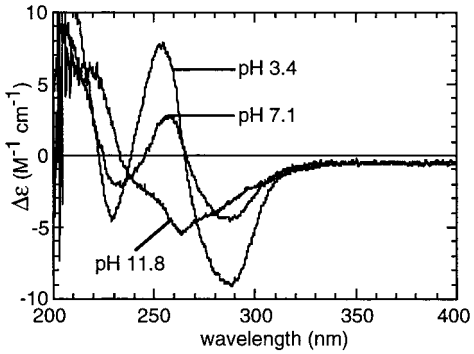

Figure 3. CD spectra of (*R,S,S,R*)-**Bip**Pt(5′-GMP)$_2$ at pH 3.4, 7.1, and 11.8, room temperature.

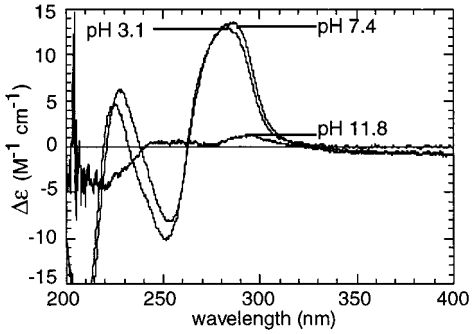

Figure 4. CD spectra of (*S,R,R,S*)-**Bip**Pt(5′-GMP)$_2$ at pH 3.1, 7.4, and 11.8, room temperature.

(∼0.1−0.15 ppm) than the HT (∼0.05 ppm) H8 signals. The ^{1}H NMR spectrum of (*S,R,R,S*)-**Bip**Pt(5′-GMP)$_2$ showed a change in the major:minor HT ratio from >25 at pH 7.4 to ∼1 at pH 11.4 (Figure 2 and Table 2). Shifts depended on pH in the fashion described above for (*R,S,S,R*)-**Bip**Pt(5′-GMP)$_2$ as follows: the HH_u and minor HT H8 signals shifted upfield more than did the HH_d and major HT H8 signals; and the H1′ or H2′ chemical shifts did not change. Because the equilibration rate is very slow at high pH and **G** H8 can exchange with D_2O, distributions at high pH are only approximate.

CD Spectroscopy. The CD spectrum of (*R,S,S,R*)-**Bip**Pt(5′-GMP)$_2$ at pH 7 closely resembles the pH 3 spectrum with negative bands at 288 and 228 nm and a positive band at 254 nm; however, the intensity of the 288 nm band was less than at pH 3 (−4.5 M^{-1} cm^{-1} at pH 7 vs −9.1 M^{-1} cm^{-1} at pH 3) (Figure 3). When the pH was raised to ∼11.8, the 288 and 254 nm peaks disappeared, and a new negative band at 262 nm was observed (Figure 3). (*S,R,R,S*)-**Bip**Pt(5′-GMP)$_2$ exhibited a similarly shaped CD signal at pH 7 but with bands opposite in sign to those of (*R,S,S,R*)-**Bip**Pt(5′-GMP)$_2$ (Figure 4). The band at 284 nm observed at pH 3 ($\Delta\epsilon = 12.5$ M^{-1} cm^{-1}) shifted to 288 nm and increased in intensity at pH 7. Between pH 7.4 and 11.8, the intensity of the 288 nm peak decreased to ∼0, and the CD spectrum at pH 11.8 had no distinct peaks (Figure 4). CD spectra of the respective isomers of the complexes of the related **CCC** C_2-symmetrical ligand, **Me$_2$DAB**Pt(5′-GMP)$_2$, have features much like those obtained for the **Bip**Pt complexes, including the same wavelength maxima/minima (±2 nm) and peak signs at pH 3.[34] CD signal shape is a clear means for assigning the chirality of the major HT form of *cis*-PtA_2**G**$_2$ complexes when that form clearly dominates.

(*S,R,R,S*)-BipPt(5′-dGMP)$_2$. The ^{1}H NMR spectrum of (*S,R,R,S*)-**Bip**Pt(5′-dGMP)$_2$ at pH 3 and 25 °C was nearly identical at equilibrium to that of the analogous 5′-GMP complex under similar conditions. Four H8 signals, one much more intense than the other three, were observed, indicating the presence of three atropisomers with major:minor HT = 7 (Table 2). Assignment of the signals and the pH dependence were essentially the same as for the analogous 5′-GMP complex. The major ΛHT rotamer had increased in abundance at pH 7.2, where it was observed almost exclusively (major:minor HT > 25) (Table 2). At high pH, the major:minor HT ratio decreased (Table 2 and Supporting Information).

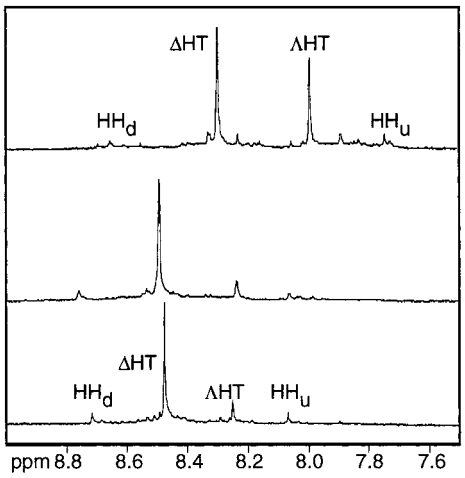

Figure 5. H8 ^{1}H NMR signals of (*R,S,S,R*)-**Bip**Pt(3′-GMP)$_2$ at (from bottom to top) pH 3.5, 7.2, and 11.5, 25 °C.

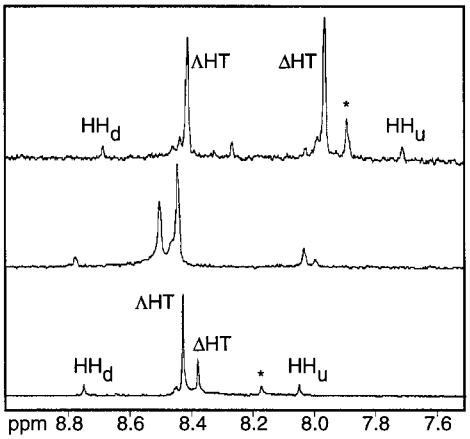

Figure 6. H8 ^{1}H NMR signals of (*S,R,R,S*)-**Bip**Pt(3′-GMP)$_2$ at (from bottom to top) pH 3, 7.7, and 11, 25 °C (∗ indicates free 3′-GMP).

(*R,S,S,R*)-BipPt(3′-GMP)$_2$ and (*S,R,R,S*)-BipPt(3′-GMP)$_2$. The ^{1}H NMR spectra of (*R,S,S,R*)-**Bip**Pt(3′-GMP)$_2$ and (*S,R,R,S*)-**Bip**Pt(3′-GMP)$_2$ at pH 3 and 25 °C were similar to the spectra of the analogous 5′-GMP complexes at equilibrium under the same conditions (Figures 5 and 6). Four H8 signals were observed in the two spectra, indicating the presence of three atropisomers in each system. One H8 signal in each spectrum was much more intense than the others and was assigned to an HT atropisomer. The most downfield and most upfield H8 signals for both 3′-GMP complexes were assigned to HH_d and HH_u as above.

HT Conformation Assignment. The H8 shift pattern and the pH behavior of the NMR and CD spectra have a distinctive signature for the 5′-GMP and 9-EtG (see below) complexes, for which we have determined the absolute conformations by NMR methods. Comparison of these properties of the 3′-GMP complexes allowed us to determine that the major HT conformations at low pH were ΔHT for (*R,S,S,R*)-**Bip**Pt(3′-GMP)$_2$ and ΛHT for (*S,R,R,S*)-**Bip**Pt(3′-GMP)$_2$. Furthermore, the absolute conformations of the **Me$_2$DAB**Pt(3′-GMP)$_2$ rotamers were

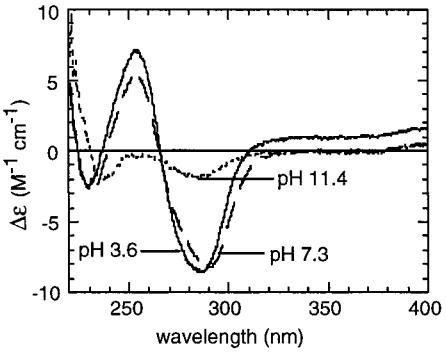

Figure 7. CD spectra of (*R,S,S,R*)-**Bip**Pt(3′-GMP)$_2$ at pH 3.6, 7.3, and 11.4, room temperature.

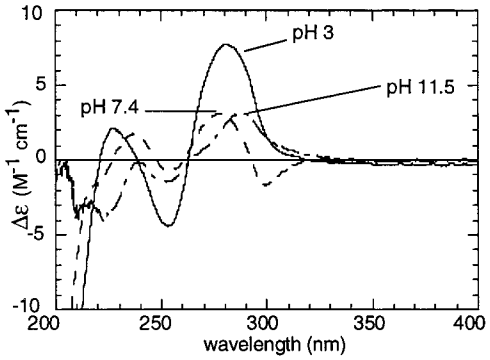

Figure 8. CD spectra of (*S,R,R,S*)-**Bip**Pt(3′-GMP)$_2$ at pH 3, 7.4, and 11.5, room temperature.

assigned using 2D NMR methods, and the wavelength maxima (±2 nm) and sign of the CD spectra of the **Bip**Pt(3′-GMP)$_2$ complexes are the same as found for the respective **Me$_2$DAB**Pt-(3′-GMP)$_2$ complexes at low pH.[34]

pH Studies. At low pH, the major:minor HT ratio was ∼7.2 for (*R,S,S,R*)-**Bip**Pt(3′-GMP)$_2$ (Table 2). The major ΔHT rotamer of (*R,S,S,R*)-**Bip**Pt(3′-GMP)$_2$ became the almost exclusively observed atropisomer at pH 7.4 (Figure 5 and Table 2). The low-pH equilibrium H8 signal intensities were again observed after lowering of the pH to 3. At pH 11.5, the major: minor HT ratio had decreased (Table 2). The H8 signals did not shift significantly until pH 8.4, where N(1)H deprotonation typically occurs in *cis*-PtA$_2$**G**$_2$ systems.[59−61] The HH$_d$ and ΔHT signals shifted upfield ∼0.1 and 0.2 ppm, respectively, from pH 7−11.5, while the ΛHT and HH$_u$ H8 signals shifted upfield ∼0.25 and 0.3 ppm, respectively.

For (*S,R,R,S*)-**Bip**Pt(3′-GMP)$_2$, from pH 3 to 12, the major: minor HT ratio decreased. The ΔHT H8 signal shifted downfield 0.15 ppm from pH 3 to 7, while the other H8 signals did not shift. From pH 7 to 11, the minor HT and HH$_u$ H8 signals, from **G**'s that can form O6−NH(**Bip**) H-bonds, shifted significantly upfield (0.5 and 0.25 ppm, respectively), while the major HT and HH$_d$ H8 signals shifted upfield only slightly (<0.1 ppm).

CD Spectroscopy. The CD spectra of (*R,S,S,R*)-**Bip**Pt(3′-GMP)$_2$ and (*S,R,R,S*)-**Bip**Pt(3′-GMP)$_2$ at pH 3 were similar in shape to those of the respective 5′-GMP complexes at pH 3. A CD pH titration of (*R,S,S,R*)-**Bip**Pt(3′-GMP)$_2$ showed that the 287 nm peak shifted to ∼290 nm between pH 3.6 and 7.3 (Figure 7). By pH 11.4, the 290 nm peak had greatly decreased in intensity, and the spectrum had no distinct bands. For (*S,R,R,S*)-**Bip**Pt(3′-GMP)$_2$, the 280 nm CD peak decreased in intensity from pH 3.1 to 7.4, and from pH 7.4 to 11.5, it shifted to ∼290 nm (Figure 8).

[*rac*-BipPt(9-EtG)$_2$]$^{2+}$. In the ^{1}H NMR spectrum of [*rac*-**Bip**Pt(9-EtG)$_2$]$^{2+}$ at pH 3.65 and 25 °C, four H8 signals,

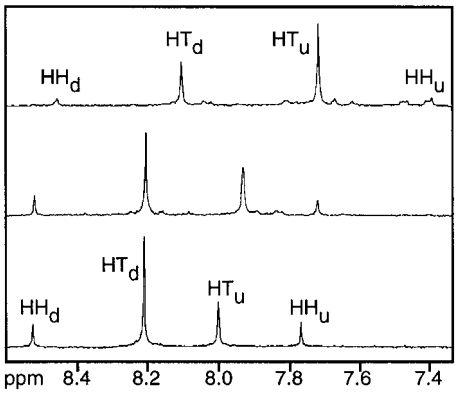

Figure 9. H8 ^{1}H NMR signals of *rac*-[**Bip**Pt(9-EtG)$_2$]$^{2+}$ at (from bottom to top) pH 3, 7.4, and 10.8, 25 °C.

observed upfield relative to the 5′-GMP and 3′-GMP complexes but in a similar pattern (Figure 9), were assigned as above. Only four H8 signals (vs eight for *rac*-**Bip**Pt(5′-GMP)$_2$) were seen because, in the absence of the sugar moiety, true HT enantiomers are present and have equivalent signals; e.g., ΛHT [(*R,S,S,R*)-**Bip**Pt(9-EtG)$_2$]$^{2+}$ and ΔHT [(*S,R,R,S*)-**Bip**Pt(9-EtG)$_2$]$^{2+}$. Therefore, the H8 signals of the [*rac*-**Bip**Pt(9-EtG)$_2$]$^{2+}$ HT atropisomers will be referred to as HT$_d$ for the downfield HT H8 signal and HT$_u$ for the upfield HT H8 signal. At equilibrium, the atropisomer with the HT$_d$ H8 signal was most abundant. The HT conformer populations were more similar at equilibrium than in the 5′-GMP or 3′-GMP adducts at low pH (Table 2).

Saturation Transfer Experiments. No exchange phenomena were observed in the [*rac*-**Bip**Pt(9-EtG)$_2$]$^{2+}$ NOESY spectrum. Saturation transfer experiments at pH 3 showed no transfer of magnetization between any atropisomer signals at 30 or 60 °C, but at 80 °C, magnetization transfer occurred from the HT$_u$ H8 signal to the HH H8 signals as well as from the HT$_d$ H8 signal to the HH H8 signals (Supporting Information). Thus, interconversion of rotamers is detectable in this system, but only at high temperature. As might be expected, there is no direct interconversion from the rotamer with the HT$_d$ H8 signal to the one with the HT$_u$ H8 signal, and the less stable minor conformer (with the HT$_u$ H8 signal) converts to the HH rotamer faster than the more stable conformer (with the HT$_d$ H8 signal) converts to the HH rotamer.

pH Studies. An NMR pH titration from pH 3 to 7 showed no significant change in the chemical shifts or intensities of the H8 signals of [*rac*-**Bip**Pt(9-EtG)$_2$]$^{2+}$ (Figure 9 and Table 2). From pH 7 to 10.8, the major:minor H8 signal ratio decreased to <1 and the HH signal intensity also decreased (Figure 9 and Table 2). The HT$_u$ and HH$_u$ H8 signals, from **G** bases that can form O6−NH H-bonds, shifted upfield more than did the HT$_d$ and HH$_d$ H8 signals over this same pH range.

[(*R,S,S,R*)-BipPt(9-EtG)$_2$]$^{2+}$ and [(*S,R,R,S*)-BipPt(9-EtG)$_2$]$^{2+}$. HT Conformation Assignment. ROESY spectra were collected using mixing times of 100 and 350 ms for [(*R,S,S,R*)-**Bip**Pt(9-EtG)$_2$]$^{2+}$. In the 100 ms mixing time ROESY spectrum, cross-peaks useful for assigning conformation were observed only for the major HT H8 signal. In the 350 ms ROESY spectrum, H8−NH cross-peaks were observed for the HH$_d$ and major HT H8 signals, as was the case in the NOESY spectrum of *rac*-**Bip**Pt(5′-GMP)$_2$. These same H8 signals also had cross-peaks to C^{6}H$_{eq}$ signals. For the HH$_d$ and major HT H8 signals, the H8−NH cross-peak volume was large, leading to the assignment of HH$_d$ to the **G** that cannot form an O6−NH hydrogen bond and of the major HT signal to the ΔHT rotamer of [(*R,S,S,R*)-**Bip**Pt(9-EtG)$_2$]$^{2+}$. In the 350 ms ROESY spectrum, the minor

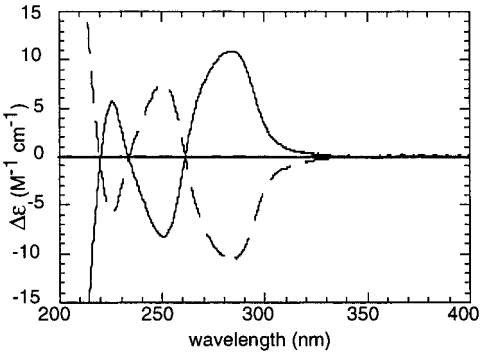

Figure 10. CD spectra of [(*R*,*S*,*S*,*R*)-**Bip**Pt(9-EtG)$_2$]$^{2+}$ (broken line) and [(*S*,*R*,*R*,*S*)-**Bip**Pt(9-EtG)$_2$]$^{2+}$ (solid line) at pH 3, room temperature.

Table 3. Energies of Minimized Structures Obtained from Molecular Dynamics and Minimization Calculations

complex	energy (kcal/mol) ΔHT	HH	ΛHT
(*R*,*S*,*S*,*R*)-**Bip**Pt(5′-GMP)$_2$	−20.27	−14.27	−17.36
(*R*,*S*,*S*,*R*)-**Bip**Pt(3′-GMP)$_2$	−22.20	−16.00	−20.20
[(*R*,*S*,*S*,*R*)-**Bip**Pt(9-EtG)$_2$]$^{2+}$	37.87	38.77	39.13
(*S*,*R*,*R*,*S*)-**Bip**Pt(5′-GMP)$_2$	−17.17	−15.68	−22.99
(*S*,*R*,*R*,*S*)-**Bip**Pt(3′-GMP)$_2$	−20.19	−14.71	−20.36
[(*S*,*R*,*R*,*S*)-**Bip**Pt(9-EtG)$_2$]$^{2+}$	38.05	38.91	37.67

HT H8 signal had no cross-peak to NH but did have cross-peaks to C^6H_{ax} and C^2H. Therefore, the minor HT atropisomer of [(*R*,*S*,*S*,*R*)-**Bip**Pt(9-EtG)$_2$]$^{2+}$ is the ΛHT conformer, which can form O6−NH hydrogen bonds. On the basis of CD spectra (see below), the major HT atropisomer of [(*S*,*R*,*R*,*S*)-**Bip**Pt(9-EtG)$_2$]$^{2+}$ has the opposite conformation from [(*R*,*S*,*S*,*R*)-**Bip**Pt-(9-EtG)$_2$]$^{2+}$ and was thus assigned the ΛHT conformation.

CD Spectroscopy. At low pH, CD signals observed for [(*R*,*S*,*S*,*R*)-**Bip**Pt(9-EtG)$_2$]$^{2+}$ and [(*S*,*R*,*R*,*S*)-**Bip**Pt(9-EtG)$_2$]$^{2+}$ were mirror images (Figure 10), as expected since all conformers are diastereoisomers. The respective conformers of 5′-GMP and 3′-GMP complexes cannot be diastereoisomers, and the respective spectra showed some slight differences in the ellipticity of the maximum at ∼285 nm. The 9-EtG complexes have CD spectra similar to those of their [**Me$_2$DAB**Pt(9-EtG)$_2$]$^{2+}$ counterparts (i.e., peaks at the same wavelength and with the same sign),[34] indicating similar absolute conformations of the favored HT atropisomer for a given secondary amine configuration regardless of **CCC** ligand.

Molecular Mechanics and Dynamics (MMD) Calculations. MMD calculations (Table 3) were done with all GMP phosphate groups protonated to mimic low-pH conditions; 500 energy-minimized structures were typically analyzed. For (*R*,*S*,*S*,*R*)-**Bip**Pt(5′-GMP)$_2$, the ΔHT rotamer, which cannot form any **G** O6−NH(**Bip**) hydrogen bonds, was computed to have several phosphate−cis-**G** hydrogen bonds (Table 4) and to be lower in energy due to lower van der Waals (vdw) and Coulombic energy terms; the calculated ΛHT and HH conformers had fewer hydrogen bonds and hence higher Coulombic energy contributions. The HH model of (*R*,*S*,*S*,*R*)-**Bip**Pt(5′-GMP)$_2$ formed one **G** O6−NH(**Bip**) hydrogen bond (Table 4). The ΛHT atropisomer of (*S*,*R*,*R*,*S*)-**Bip**Pt(5′-GMP)$_2$, also incapable of forming **G** O6−NH(**Bip**) hydrogen bonds, was computed to be the lowest-energy rotamer and to have two **G** PO−NH(**Bip**) and two **G** POH−O6 hydrogen bonds (Table 4). The energy difference between the two HT models of (*S*,*R*,*R*,*S*)-**Bip**Pt(5′-GMP)$_2$ was manifested mainly in higher angle and torsion angle energy terms for the ΔHT atropisomer, while the HH adduct was higher in energy than both HT rotamers primarily because of less favorable Coulombic interactions due to the presence of fewer hydrogen bonds. The HH model of (*S*,*R*,*R*,*S*)-**Bip**Pt(5′-GMP)$_2$ formed one **G** O6−NH(**Bip**) hydrogen bond. Of the HT atropisomers capable of forming **G** O6−NH(**Bip**) hydrogen bonds, the minimum energy structure(s) did not show this interaction.

The ΔHT atropisomer of (*R*,*S*,*S*,*R*)-**Bip**Pt(3′-GMP)$_2$ was computed to be more stable than the ΛHT and the HH rotamers (Table 3) due to favorable angle, torsion angle, and Coulombic energy terms. The higher Coulombic energy term again is related to the number of hydrogen bonds (Table 4). For (*S*,*R*,*R*,*S*)-**Bip**Pt-(3′-GMP)$_2$, the ΛHT and ΔHT atropisomers were computed to be almost equal in energy and to be significantly more stable than the HH model. Again, the differences were manifested chiefly in the Coulombic and torsion angle energy terms.

For [(*R*,*S*,*S*,*R*)-**Bip**Pt(9-EtG)$_2$]$^{2+}$, the ΔHT rotamer was computed to be most stable (Table 3). The ΛHT model with the lowest energy did not have **G** O6−NH(**Bip**) hydrogen bonds. Compared to this structure, one computed to form two **G** O6−NH(**Bip**) hydrogen bonds had ∼2 kcal/mol higher energy, primarily from less favorable torsion angle and vdw energy terms. For [(*S*,*R*,*R*,*S*)-**Bip**Pt(9-EtG)$_2$]$^{2+}$, the ΛHT model was most stable (Table 3). Again, no **G** O6−NH(**Bip**) H-bonds formed in the low-energy ΔHT model; a ΔHT model with two **G** O6−NH(**Bip**) hydrogen bonds was ∼4 kcal/mol less stable, primarily due to higher torsion angle and vdw energy terms. Similar Coulombic energy terms were computed for all of the 9-EtG conformers; this observation supports the interpretation given above that differences in this term arise from differences in hydrogen bonding of the sugar and the phosphate groups to the *cis*-**G** and/or NH(**Bip**).

Table 4. Hydrogen Bonds in (*R*,*S*,*S*,*R*)-**Bip**Pt**G**$_2$ and (*S*,*R*,*R*,*S*)-**Bip**Pt**G**$_2$ Model Structures[a]

(*R*,*S*,*S*,*R*)-**Bip**Pt**G**$_2$			(*S*,*R*,*R*,*S*)-**Bip**Pt**G**$_2$		
ΔHT	HH	ΛHT	ΔHT	HH	ΛHT
			5′-GMP		
PO−N(1)H (2)	O6−NH (1)	PO−N(1)H (2)	PO−N(1)H (1)	PO−3′-HO (1)	PO−NH (2)
PO−NH$_2$ (2)	PO−HOP (2)	PO−NH$_2$ (2)	PO−NH$_2$ (1)		POH−O6 (2)
POH−O6 (2)		POH−O6 (1)	POH−O6 (1)		
			PO−NH (1)		
			3′-GMP		
PO−NH$_2$ (2)	O6−NH (1)	PO−NH$_2$ (2)	PO−NH$_2$ (2)	PO−NH$_2$ (1)	PO−NH$_2$ (1)
PO−N(1)H (2)	PO−5′-HO (2)	PO−N(1)H (2)	PO−N(1)H (2)	PO−N(1)H (1)	PO−N(1)H (1)
5′-OH−O6 (2)	PO−2′-HO (2i)	PO−3′-HO (2)	PO−5′-HO (2i)	O6−NH (1)	PO−2′-HO (2i)
PO−2′-HO (2i)	PO−HOP (2)			PO−2′-HO (2i)	5′-OH−5′-O (1)
				POH−2′-OH (2i)	
				5′-O−5′-HO (1)	

[a] Number in parentheses indicates number of that type of hydrogen bond; an "i" indicates that it is an intramolecular hydrogen bond within a **G** residue.

Discussion

General Considerations. Although our results involve a broad range of conditions and several **G** derivatives, we have developed a comprehensive explanation interrelating structure, energetics, and dynamics. Before discussing the specific results for each **G** derivative, we present in general terms the interrelated components of our explanation.

Factors Controlling Dynamics. The C_2-symmetrical **CCC** carrier ligands (Chart 3) decrease dynamic motion relative to typical *cis*-PtA_2**G**$_2$ adducts. The **Bip**Pt**G**$_2$ complexes have much slower Pt−N7 rotation rates than any previously studied such adduct with two secondary amines. We attribute this effect to the rigidity of the **Bip** ligand; this rigidity has two components. First, the chelate ring is part of a three-ring system, decreasing its fluxional character relative to the related **CCC** C_2-symmetrical **Me$_2$DAB** ligand (Chart 3). Second, the CH groups projecting toward the **G** coordination sites are unable to rotate away from the **G** bases during **G** rotation around the Pt−N7 bond. In contrast, these CH's in **Me$_2$DAB** are in *N*-methyl groups, which are able to rotate freely, in essence acting as a turnstile that permits the **G** O6 to pass by easily during **G** rotation, accounting for the more rapid dynamic motion in **Me$_2$DAB**Pt**G**$_2$ complexes.[34] The *cis*-$(NH_3)_2$ groups in the anticancer drug can each act as a turnstile, contributing to the fluxional nature of *cis*-Pt$(NH_3)_2$**G**$_2$ adducts. Certainly, in addition to complete rotation, there is a thermal wagging motion of the **G** bases about the Pt−N7 bond in all cases, including the **Bip**Pt**G**$_2$ complexes (see below).

Influence of Bip Configuration on HT Chirality. The absolute conformations of the major (**CCC**)Pt**G**$_2$ HT atropisomers found by 2D NMR spectroscopy with high-field NMR instruments agree for the analogues with **CCC** = **Me$_2$DAB** or **Bip** for a given *R,S,S,R* or *S,R,R,S* configuration.[34] The evidence that the chirality at N dictates the same preferred conformations of **Me$_2$DAB**Pt**G**$_2$ and **Bip**Pt**G**$_2$ compounds at pH $\leq$ 4 has three components for any given **G**: (a) similar H8 ^{1}H NMR chemical shift values; (b) comparable equilibrium population distributions; and (c) similar CD spectra. The *R,S,S,R* chirality of **Bip** or **Me$_2$DAB** favors the ΔHT conformation, while the *S,R,R,S* chirality favors the ΛHT conformation. The MMD calculations (Table 3) correctly predict the preferred HT conformation. In all cases, the major HT rotamer at low pH cannot form **G** O6−NH(**Bip**) hydrogen bonds because the **G** O6 is on the opposite side of the coordination plane from the NH; thus, interaction between **G** O6 and NH(**Bip**) is not of great importance at low pH. Interactions involving the N9 substituents are of secondary importance (see below).

Factors Favoring the HT over the HH Conformation. For all (**CCC**)Pt**G**$_2$ systems, including **Bip**Pt**G**$_2$ complexes studied here, three atropisomers were observed at equilibrium; one HT atropisomer is dominant at low to neutral pH, and the HT:HH ratio has always been clearly >1. A preference for HT conformers has been observed for **pipen**Pt**G**$_2$ compounds (**pipen** = the hybrid primary/secondary diamine ligand, 2-aminomethylpiperidine, Chart 3).[32,33] When not connected by a phosphodiester bridge, **G** moieties are believed to adopt an HT arrangement of the bases.[23] We attribute the preferential formation of HT rotamers in all simple *cis*-PtA_2**G**$_2$ complexes to the more favorable alignment of the **G** dipoles in the HT forms than in the HH form. The binding by N7 to Pt(II) will lead to donation of electron density from the **G** imidazole ring to the metal. This interaction will in turn make the N_2CH proton, already electron deficient and bearing a partial positive charge,[39] even more positive. Since the H8's are near each other in an HH form, repulsion between these partially positive H8's will destabilize the HH form. Also in turn, the **G** dipole will be increased by the binding to Pt; this increased dipole will enhance the importance of dipole−dipole interactions between the **G**'s, favoring the HT alignment of **G** dipoles. As stated above, the chirality of the HT conformers is primarily influenced by the **CCC** ligand chirality.

Characteristics of the HT Subforms. In Chart 1, we showed two subforms for each HT chirality, Δ and Λ, or a total of four HT subforms. In the simplest dynamic compounds, e.g., *cis*-$[Pt(NH_3)_2(9\text{-EtG})_2]^{2+}$, with neither the carrier ligand nor the 9-EtG having an asymmetric center, ΔHT and ΛHT rotamers constitute an enantiomeric pair. NMR spectroscopy cannot distinguish between them. Most studies, however, have involved complexes of **G** derivatives bearing an asymmetric sugar. In these cases, NMR spectroscopy should be able to distinguish between HT conformers. As mentioned in the Introduction, the rate of conformer interchange is too great to differentiate between ΔHT and ΛHT conformers for simple *cis*-Pt$(NH_3)_2$**G**$_2$ complexes. Solid state structural data indicate that base tilting can have two different directions, right-hand (R) and left-hand (L).[14,20,34] HT isomers are clustered into two groups differing in degree of base tilt, either a ΔHTR and ΛHTL less tilted group or a ΔHTL and ΛHTR more tilted group. All four HT subforms are distinct and, in principle, resolvable by NMR spectroscopy when **G** has an asymmetric sugar. We believe that the barrier between subforms with the same HT chirality is very low and subforms cannot be observed by NMR spectroscopy due to a rapid dynamic wagging motion. Thus when the carrier ligand is bulky, only one H8 signal is observed for each HT chirality.

For a given **CCC** configuration, our observations (next paragraph) provide a clear indication of the dominance of just two subforms, one for each HT chirality. Our spectral results reflect an average of the subforms, weighted toward the energetically favored subform for each HT chirality. Thus, just two HT H8 signals are observed for each **CCC** configuration. If we do not consider the chirality of the carrier ligand, the four identifiable HT subforms are those shown in Chart 1. But in Chart 1 we have also specified the chirality of the carrier ligand that favors a particular pair of subforms.

The HT H8 signal pattern for all of the **Bip**Pt**G**$_2$ complexes, with the major HT H8 signal downfield and the minor HT H8 signal upfield, was also found and interpreted for the **Me$_2$DAB**-Pt**G**$_2$ complexes.[34] The results for both types of (**CCC**)Pt**G**$_2$ adducts can be interpreted in exactly the same way. The bases of the major and minor HT and the HH rotamers of (*R,S,S,R*)-**Bip**Pt**G**$_2$ adducts all have a right-handed tilt, while the bases in all rotamers of (*S,R,R,S*)-**Bip**Pt**G**$_2$ adducts have a left-handed tilt (Chart 1). The minor HT form has a greater tilt of the **G** bases due to the positioning needed to form **G** O6−NH(**Bip**) hydrogen bonds; this greater tilt leads to greater H8 shielding by the *cis*-**G**. The HH adducts have one base tilted more than the other, leading to the large H8 signal dispersion in this conformer (Chart 1).

The interpretation of the dependence of the H8 shift on tilt relies on the solid state structural data. Insightful calculations[20] suggested that the mutual shielding of H8 by the *cis*-**G** is greater in the more tilted form by an amount that quantitatively compares favorably to the difference in shift values we observe experimentally for the two HT forms of (**CCC**)Pt**G**$_2$ complexes.[34] Until our work with (**CCC**)Pt**G**$_2$ complexes,[34] this anisotropic effect was not documented experimentally for HT forms. Although the calculated anisotropy effect can also explain the chemical shift dispersion quantitatively for typical HH *cis*-

PtA_2(d(GpG)) adducts,[20] it cannot explain the chemical shifts of the HH (**CCC**)Pt$\mathbf{G}_2$ or (**CCC**)Pt(d(GpG))adducts.[13,19,34,36]

Factors Influencing Subform Stability. Above we discussed how **G**(dipole)−**G**(dipole) interactions favor HT over HH forms. Likewise, the observation that the less tilted "major" HT atropisomer is generally more stable than the more tilted "minor" HT atropisomer can be understood from a simplified analysis of the **G**(dipole)−**G**(dipole) interactions. In some cases, the tilt may be negligibly small, but for convenience we shall simply use the term less tilted. When we discuss the four HT subforms observed experimentally (Chart 1) in the next paragraph, we do not refer to HT chirality since the arguments are independent of chirality.

For the less tilted form, the positive H8 end of the dipole is closer to the negative six-membered ring of the *cis*-**G** base than in the more tilted form; this is the main reason that the less tilted form is favored. The mutual distances between the H8's and between the six-membered rings are at an intermediate length. The H8's are pointing toward the axial direction, away from the C_2-axis between the two **G** bases. Hence, shielding from the *cis*-**G** is small. For the more tilted HT form observed, the H8's are nearer the equatorial plane of the complex, closer to the C_2-axis between the two **G** bases. Hence, shielding from the *cis*-**G** is large (Chart 1). The distance between the H8's is short and thus unfavorable, while the distance between the six-membered rings is long, thus favorable. However, the positive H8 end of the dipole is farther from the negative six-membered ring of the *cis*-**G** base; this feature is the main reason the more tilted form is destabilized relative to the less tilted form. However, this diminished favorable energy contribution of the dipole interaction might be compensated for by a favorable energy contribution from **G** O6−NH(**Bip**) hydrogen bonding that the greater tilt allows. For the low and neutral pH forms, we believe that H-bonding involving **G** O6 and the **Bip** NH is somewhat weak compared to other interactions since (a) the less tilted conformer always predominates at pH 3; (b) such H-bonding does not even appear in some MMD models; and (c) it cannot offset some effects of the N9 substituents on distribution.

This reasoning derives support from our evaluation of the effect of pH on atropisomer stability and properties. N(1)H deprotonation of the guanine six-membered ring will increase electron density on O6, making **G** O6 a better hydrogen-bond acceptor, an explanation invoked to account for the downfield shift of NH signals for Pt(dien)(5′-GMP) at pH 9.[65] Indeed, although the situation is influenced by the N9 substituent, the redistribution of rotamers at high pH to be discussed below indicates that N(1)H deprotonation favors the "minor" HT atropisomer, which can form **G** O6−NH(**Bip**) H-bonds more favorably than before deprotonation. N(1)H deprotonation increases the **G** polarity. Since the distance between the six-membered rings is longer in the more tilted form, N(1)H deprotonation will also favor the more tilted form since the resulting N1 negative charges are better separated. Likewise, the H8 will probably have somewhat less partial positive charge; the unfavorable H8−H8 repulsion will be less. In contrast, the attraction of the positive end toward the negative end of the dipole, an attraction favoring the less tilted form, will be increased. On balance, the changes in the forces on deprotonation of N(1)H will favor the more tilted form.

Dependence of Rotamer Distribution on Properties of the G Ligands. The four **G**'s used in this study each have different N9 substituents and thus different potential interactions between these substituents and the **Bip** and the *cis*-**G** ligands. Although these interactions are secondary to those between the **G** bases arising from the dipole alignments and those between the **G** base and the chiral **Bip** ligand, the N9 substituents do have some modulating influence on the atropisomer distribution. We can interpret many of the ways that the interactions of the N9 substituents with the **Bip** and the *cis*-**G** ligands influence rotamer distribution. The simplest **G** derivative, 9-EtG, can form only **G** O6−NH(**Bip**) hydrogen bonds. 3′-GMP can form **G** O6−NH(**Bip**) and **G** phosphate−*cis*-**G** hydrogen bonds. The 3′-phosphate groups can also be involved in phosphate-phosphate repulsion or electrostatic attraction to the positive charge resulting from the Pt(II) center. 5′-GMP and 5′-dGMP have the same potential interactions as 3′-GMP, with the added possibility of forming **G** PO−NH(**Bip**) hydrogen bonds (5′-dGMP has no 2′-OH to form additional hydrogen bonds to the cis 5′-dGMP). We shall begin with characterization of the simplest system and continue to increasingly more complicated systems.

Since, in a few of the cases to be discussed next, the "major" HT conformer favored at low pH became less abundant than the "minor" HT atropisomer at high pH, we suggest that the reader recall a simple rule: If the **CCC** ligand N configuration is *R* (e.g., *R,S,S,R*), the "major" HT form that is favored at low to neutral pH is Δ and right-handed. For an *S* nitrogen, a Λ left-handed "major" form is favored. Since *R*, Δ, and right-handed all connote "right" in a loose sense, this relationship should be easy to remember.

G = 9-EtG. At low pH, the major HT rotamer of [(*R,S,S,R*)-**Bip**Pt(9-EtG)$_2$]$^{2+}$ or [(*S,R,R,S*)-**Bip**Pt(9-EtG)$_2$]$^{2+}$ cannot form **G** O6−NH(**Bip**) hydrogen bonds. As the pH was raised to deprotonate **G** N(1)H, the major form at low pH became less abundant than the "minor" form (Figure 9 and Table 2). For all **Bip**Pt$\mathbf{G}_2$ complexes studied here, the "major" form at low pH becomes less favored at high pH.

G = 3′-GMP. Between pH 3 and 7, the 3′-phosphate group deprotonates, and the ΔHT rotamer increases in abundance for (*R,S,S,R*)-**Bip**Pt(3′-GMP)$_2$ and (*S,R,R,S*)-**Bip**Pt(3′-GMP)$_2$ (Figures 5 and 6). For non-**CCC** carrier ligands, 3′-GMP favors the ΔHT atropisomer, particularly at pH 7.[32] For (**CCC**)Pt$\mathbf{G}_2$ complexes, according to the *R*, Δ, right-handed tilting rule, the (*R,S,S,R*)-**CCC** ligand chirality stabilizes the ΔHT conformer.[34] These biases both favor the ΔHT conformer and contribute to the very high ΔHT rotamer population of 95% at pH 7 for (*R,S,S,R*)-**Bip**Pt(3′-GMP)$_2$. The 3′-phosphate group is too far removed from the Pt atom for strong electrostatic interaction, and a similar electrostatic interaction would be possible for the ΛHT rotamers. The likely role that the phosphate plays in favoring the ΔHT conformation is formation of phosphate−*cis*-**G** H-bonds; such H-bonds are present in the models of lowest energy of these ΔHT rotamers (Table 4), and these H-bonds should be strongest at pH 7. The ΔHT rotamer of (*S,R,R,S*)-**Bip**Pt(3′-GMP)$_2$ has less tilted bases after phosphate deprotonation, as evidenced by the downfield shift of the ΔHT H8 signal (Figure 6). For (*S,R,R,S*)-**Bip**Pt(3′-GMP)$_2$, the lesser tilt of the bases and the phosphate−*cis*-**G** hydrogen bonding both contribute to stabilizing the ΔHT conformer.

From pH 3 to 7, the intensity of the CD signal at ∼284 nm did not change much for (*R,S,S,R*)-**Bip**Pt(3′-GMP)$_2$ and decreased for (*S,R,R,S*)-**Bip**Pt(3′-GMP)$_2$ (Figures 7 and 8). In the case of (*R,S,S,R*)-**Bip**Pt(3′-GMP)$_2$, the ΔHT atropisomer is essentially the only species from pH 3 to 7. Thus, the minimal change in the CD signal reflects the predominance of the ΔHT rotamer. For (*S,R,R,S*)-**Bip**Pt(3′-GMP)$_2$, the ΛHT rotamer is the

(65) Guo, Z.; Sadler, P. J.; Zang, E. *Chem. Commun.* **1997**, 27.

major conformer from pH 3 to 7, but it has greatly decreased in abundance by pH 7 relative to the ΔHT rotamer (Table 2). The decreased intensity of the "Λ" CD spectrum most likely reflects the decreased amount of the ΛHT atropisomer.

The pH dependence of the CD spectra and the rotamer distribution (as determined by NMR spectra) observed for (*R,S,S,R*)- and (*S,R,R,S*)-**Bip**Pt(3′-GMP)$_2$ from pH 3 to ∼7 are similar to those found for (*R,S,S,R*)- and (*S,R,R,S*)-**Me$_2$DAB**Pt(3′-GMP)$_2$ and (*R,S*)- and (*S,R*)-**pipen**Pt(3′-GMP)$_2$.[19,32] In all cases, the ΔHT form has a greater population than expected relative to the analogues with other **G** ligands. These results suggest that phosphate−*cis*-3′-GMP interactions favor the ΔHT rotamer regardless of secondary amine chirality.

G = 5′-GMP and 5′-dGMP. Similar CD experiments on 5′-GMP complexes with non-**CCC** ligands, as described above for 3′-GMP complexes, gave evidence indicating that *cis*-PtA$_2$(5′-GMP)$_2$ complexes favor the ΛHT conformation at pH's below N(1)H deprotonation.[32] An assessment of the role of the 5′-phosphate group in influencing rotamer preference from pH 3 to 7 is complicated by the larger conformational space the 5′-phosphate group can occupy compared to the 3′-phosphate group. However, all of our results (Figures 1 and 2, for 5′-dGMP see Supporting Information) suggest that favorable phosphate−*cis*-**G** hydrogen bonds stabilize the ΛHT form for 5′-GMP from pH 3 to 7.

However, this *cis*-**G** effect is not so clear in the 5′-GMP case as in the 3′-GMP case. The 5′-phosphate group can reach the carrier ligand NH and form hydrogen bonds. In addition, the phosphate group in this position is in the vicinity of the positive Pt(II) center, further favoring interaction with the carrier ligand. For 5′-GMP complexes with (*S,R,R,S*)-**Bip**, (*S,R,R,S*)-**Me$_2$DAB**, or (*S,R*)-**pipen** ligand, the ΛHT rotamer increased from pH 3 to 7.[32] Both carrier ligand configuration and phosphate−*cis*-**G** and/or phosphate−NH hydrogen bonds favor the ΛHT form, accounting for the high abundance of the ΛHT atropisomer of (*S,R,R,S*)-**Bip**Pt(5′-GMP)$_2$ at pH 7 (Table 2). For the (*R,S,S,R*)-**Bip** and (*R,S,S,R*)-**Me$_2$DAB** complexes, the major ΔHT atropisomer, favored by the *R* configuration of the secondary amine, remained the dominant species, but the ΛHT rotamer increased in abundance from pH 3 to 7. This result indicates that even for 5′-GMP the phosphate interaction with the *cis*-**G** in the ΛHT form is favored over the interaction with the *cis*-NH in the ΔHT form. However, for the (*R,S*)-**pipen** complex, the two interactions appear to balance each other, and the HT ratio does not change significantly from pH 3 to 7.

For both (*R,S,S,R*)-**Bip**Pt(5′-GMP)$_2$ and (*S,R,R,S*)-**Bip**Pt(5′-GMP)$_2$, the HH rotamer is more abundant than the minor HT atropisomer at equilibrium; this relationship was also found for **Me$_2$DAB**Pt(5′-GMP)$_2$ complexes.[34] The minor HT conformer was more abundant than the HH rotamer for **Bip**Pt**G**$_2$ and **Me$_2$DAB**Pt**G**$_2$ complexes with **G** = 9-EtG and 3′-GMP.[34] For 5′-GMP, the HH atropisomer can have one **G** O6−NH(**Bip**) and one phosphate−NH(**Bip**) H-bond; the second H-bond is not possible for 3′-GMP or 9-EtG. This second hydrogen bond increases the stability of the HH atropisomer in the 5′-GMP systems.

G H8 Shifts. The H8 signals of **G**'s that are more tilted and positioned for **G** O6−NH(**Bip**) hydrogen bonding, e.g., HH$_u$ and HT$_u$ H8 signals of 9-EtG, shift upfield more upon N(1)H deprotonation than do the signals of the less tilted **G**'s, e.g., HH$_d$ and HT$_d$ H8 signals of 9-EtG, although all H8 signals generally shift upfield with N(1)H deprotonation (Figures 1, 2, 5, 6, and 9).[34,40,61,64] This observation can be taken as evidence that N(1)H-deprotonated **G** bases adopt on average a more tilted orientation to allow **G** O6−NH(**Bip**) hydrogen bonding. Alternatively, the upfield shifts may be due not to a change in tilting but to the electronic effects of deprotonation of N(1)H. For example, the anisotropy of the **G** base may decrease, causing less deshielding of H8; however, if this were the main factor, it is difficult to explain the small effect on the H8 shift of the less tilted **G**'s. Also, Pt anisotropy can influence the shifts in a geometrically dependent manner.[66] Donation of electron density from the deprotonated **G**'s will change the metal anisotropy and influence the H8 shift of tilted and less tilted **G**'s differently. At present, we favor the explanation that deprotonation increases the average tilt since this explanation accounts for both the large upfield shifts and the greater stability of rotamers that can form **G** O6−NH(**Bip**) hydrogen bonds.

Summary. The favorable alignment of the **G** dipoles in the two HT rotamers stabilizes these two rotamers vs the HH rotamer of **Bip**Pt**G**$_2$ complexes. For a given **Bip** configuration, all three **Bip**Pt**G**$_2$ rotamers have the same tilt direction. One **Bip**Pt**G**$_2$ HT rotamer, the "major" HT rotamer, is preferred at equilibrium. The chirality of this major HT rotamer and the tilt direction are dictated by the **Bip** secondary amine configuration. The *R,S,S,R* configuration leads to a ΔHT major rotamer with right-handed tilt, whereas the *S,R,R,S,* configuration leads to a left-handed tilted ΛHT major rotamer. For each **Bip** configuration, the major atropisomer has less tilted bases and no **G** O6−NH(**Bip**) hydrogen bonding. The more favorable dipole−dipole interaction in a less tilted arrangement for the major HT rotamer could offset the combined contributions of **G** O6−NH(**Bip**) hydrogen bonding and less favorable dipole−dipole interactions in the more tilted arrangement of the minor HT form.

In addition to **G**−**Bip** and **G** base−**G** base interactions, other factors affect the atropisomer population. These are revealed by changes in solution pH and the **G** N9 substituent. At pH 7, interactions between the phosphate group of one **G** and the *cis*-**G** are clearly more favorable in the ΔHT form of 3′-GMP complexes and somewhat more favorable in the ΛHT form of 5′-GMP complexes. When **G** N(1)H is deprotonated, **G** O6−NH(**Bip**) hydrogen bonding becomes important and favors the minor HT form; this effect is most evident in 9-EtG complexes. However, for GMP complexes, **G** N(1)H deprotonation leads to repulsive forces between the trinegative *cis*-**G** nucleotides. These repulsive forces favor the ΛHT form for 3′-GMP and the ΔHT form for 5′-GMP and can enhance or oppose the effects of **G** O6−NH(**Bip**) hydrogen bonding.

Acknowledgment. This work was supported by NIH Grant GM 29222 (to L.G.M.) and NATO CRG 950376 (to L.G.M. and G.N.); MURST (Contribution 40%), CNR, and EC (COST Chemistry project D8/0012/97 (to G.N.)).

Supporting Information Available: Partial 2D NMR, partial 1D ^{1}H NMR pH titration, and saturation transfer data. This material is available free of charge via the Internet at http://pubs.acs.org.

IC981409G

(66) Sundquist, W. I.; Bancroft, D. P.; Lippard, S. J. *J. Am. Chem. Soc.* **1990**, *112*, 1590.